Influence of Pt Addition and Manufacturing Process on the Failure Mechanisms of NiCoCrAlYTa-Base Thermal Barrier Coating Systems under Thermal Cycling Conditions

Aurelie Vande Put [1],*, Djar Oquab [1], Aymeric Raffaitin [2] and Daniel Monceau [1]

[1] Centre Interuniversitaire de Recherche et d'Ingénierie des Matériaux (CIRIMAT), Université de Toulouse, CNRS, INP-ENSIACET 4 allée Emile Monso-BP44362, 31030 Toulouse CEDEX 4, France; djar.oquab@ensiacet.fr (D.O.); daniel.monceau@ensiacet.fr (D.M.)

[2] Safran Helicopter Engines, Avenue Joseph Szydlowski, 64510 Bordes, France; raffaitina@yahoo.fr

* Correspondence: aurelie.vandeput@ensiacet.fr; Tel.: +33-5-3432-3416

Abstract: The cyclic oxidation of NiCoCrAlYTa-base thermal barrier coating systems was investigated at 1100 °C. The influence of the NiCoCrAlYTa deposition process, the coating modification by a Pt-overlayer, and the surface preparation steps were studied. Thermal cycling results showed that the addition of a Pt-overlayer, a dense and oxide-free bond-coating microstructure, together with a smooth NiCoCrAlYTa surface prior to Pt deposition and a suitable surface preparation before thermal barrier deposition all increase the lifetime. Degradation mechanisms are proposed to explain how coating defects develop during thermal cycling and how the fabrication process influences both failure and lifetime.

Keywords: TBC system; MCrAlY; oxidation; platinum

1. Introduction

Thermal barrier coating (TBC) systems have been developed to reduce the temperature of turbine blades. They consist of a Ni-base superalloy (the blade), an Al-rich coating (the bond-coating, BC) and an insulating top coat (TBC) made of yttria-stabilized zirconia (YSZ). For aeronautic applications, the top coat is usually deposited by electron-beam physical vapor deposition (EB-PVD) to obtain a columnar microstructure, making it capable of accommodating strain. Because YSZ is permeable to oxygen, it cannot protect the superalloy against oxidation. To ensure protection, the Al-rich bond-coating has to form a layer of α-Al$_2$O$_3$, a protective, adherent and slow-growing oxide, called thermally grown oxide (TGO).

In service, TBC systems undergo mechanical and environmental stresses under high temperatures. Whether it is due to foreign object damage [1,2], calcium–magnesium–aluminosilicate (CMAS) deposition [3,4] or thermo-mechanical damage of the TBC system [5], environmental stresses lead to damage and/or loss of the thermal barrier, which is harmful for the TBC system lifetime. A key point of TBC system thermo-mechanical damage is TGO formation and growth. Indeed, this oxide scale, forming between the bond-coating and the TBC, undergoes stresses resulting from: (i) the transformation from transient alumina to α-alumina; (ii) the oxide growth, and (iii) the thermal expansion coefficient (CTE) mismatch. While the transient alumina to α-alumina transformation leads to tensile stresses [6,7], the other two phenomena result in compressive stresses. Due to a great difference between the alumina volume and the volume of consumed metal, compressive stresses reaching 200 MPa at 1100 °C could be generated within the oxide scale [7]. Regarding

material CTE, it is equal to 8–9 ppm/°C and 13–16 ppm/°C for alumina and the bond-coating respectively [5]. During cooling, the oxide scale is then under compressive stresses, contained between 2.5 and 4 GPa [8]. Heterogeneities in oxide composition, thickness, or flatness add stresses within the TGO and consequently favor crack initiation and TBC damage. Studying the oxide resistance of bond-coatings and TBC systems is therefore important to improve the lifetime of such systems.

Three main bond-coatings in use are: the Pt-modified β-NiAl, the Pt-rich γ-Ni + γ'-Ni$_3$Al, and the MCrAlY (where M = Ni and/or Co) coatings. With their composition rich in Cr and Al, MCrAlY coatings have a good resistance against high temperature corrosion [9–11]. They generally out-perform Pt-modified β-NiAl aluminides against type-I and type-II hot corrosion [12], corrosion due to salt contaminants such as Na$_2$SO$_4$, NaCl, V$_2$O$_5$ [13]. Moreover, they contain yttrium, a reactive element beneficial for TGO adherence [14]. However, MCrAlY coatings do not behave as well as Pt-modified aluminide coatings under oxidizing conditions as they can form chromia and spinel oxides in addition to the continuous Al$_2$O$_3$ layer. To improve their oxidation and corrosion resistance, Pt was added [10,15–29]. Pt addition to MCrAlY coatings was also beneficial in terms of TBC system lifetime [20,22,30,31].

First, attention was focused on the influence of Pt addition on the microstructure of NiCoCrAlYTa bond-coatings [32], and then on the oxidation behavior of Tribomet® NiCoCrAlYTa bond-coatings [23]. With this work, the effect of Pt on the degradation mechanism of TBC systems containing a NiCoCrAlYTa bond-coating under cyclic oxidation conditions was studied. The present study also considers the influence of the deposition process and the surface preparation of the NiCoCrAlYTa coating, well known parameters that affect the TBC system lifetime.

2. Materials and Methods

To study the effect of Pt addition on the degradation mechanisms of TBC systems with a NiCoCrAlYTa bond-coating, two samples were manufactured, one with and one without Pt. To understand the influence of the bond-coating fabrication process, NiCoCrAlYTa coatings were made either by composite electroplating (Tribomet® process) or vacuum plasma spray (VPS).

2.1. Materials and Coatings

Three Ni-base superalloys were used for the fabrication of the TBC systems: the 1st generation superalloy AM3, the 2nd generation superalloy CMSX-4, and the 4th generation superalloy MCNG. CMSX-4 superalloy contains Re and some Hf, as MCNG superalloy which also contains Ru. Their compositions are given in Table 1.
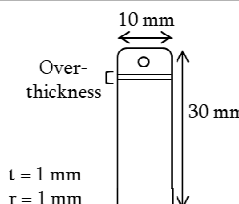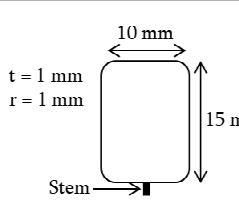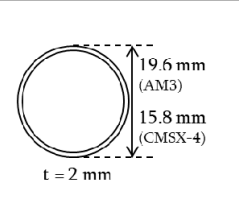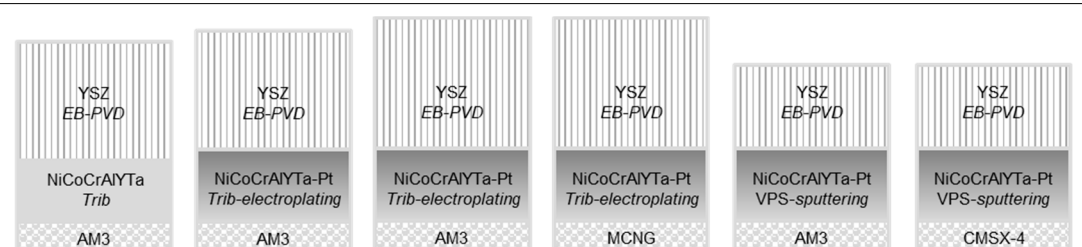
Table 1. Superalloy composition. The Hf concentration of CMSX-4 superalloy was measured by glow discharge mass spectroscopy (GDMS) by Shiva Technology, as well as the sulfur content.

At %	Ni	Al	Cr	Co	Ta	Ti	Mo	W	Re	Ru	Others
AM3	Bal.	12.9	8.9	5.9	1.3	2.4	1.2	1.6	-	-	S: Batch 2: <0.5 ppmw, Batch 3: 0.28 ppmw, Hf free
CMSX-4	Bal.	12.6	7.6	9.9	2.2	1.3	0.4	2.2	1.0	-	0.67 ppmw Hf, 1.4 ppmw S
MCNG	Bal.	13.6	4.7	-	1.7	0.6	0.6	1.7	1.3	2.4	0.03 at % Hf, 0.16 ppmw S

Three batches of NiCoCrAlYTa-base TBC systems were manufactured. The NiCoCrAlYTa coating was made using either the Tribomet® process (Praxair ST, Oldmixon, UK) or vacuum plasma spraying (Surface Engineering Research Laboratory, LERMPS, Montbéliard, France), while Pt was deposited either by electroplating (Praxair ST, Indianapolis, IN, USA) or by sputtering (Cranfield University, Bedfordshire, England, UK). The thermal barrier was always deposited by EB-PVD but by various manufacturers: Praxair ST (Indianapolis, IN, USA), Ceramic Coating Center (Châtellerault, France), and Surface Engineering and Nanotechnology Institute (Cranfield University, England). All the details regarding the specimen geometry, the deposition techniques, the thicknesses, the surface preparations,

and the manufacturers are given in Table 2. The first batch was provided by Praxair ST and was composed of AM3-base TBC systems both with and without Pt. To coat the entire surface of the rectangular AM3 specimens with NiCoCrAlYTa coating, two passes were required, generating a locally thicker coating. In addition, a hole was drilled at one end of the AM3 substrate to coat the entire sample surface with the thermal barrier. The fabrication of the second batch, on AM3 and MCNG superalloys, involved Praxair ST for the bond-coating and Ceramic Coating Center for the thermal barrier. A stem made of Hastelloy W was welded to one edge of the rectangular substrate in order to hold the sample during the coating process. This allowed the deposition of a uniform coating. For batch 3, only one face of the substrate was coated. The manufacturing of the VPS NiCoCrAlYTa coating was performed at LERMPS using AMDRY 997 powder (wt %: Ni-23Co-20Cr-8.5Al-4Ta-0.6Y; at %: Ni-20.9Co-20.9Cr-16.9Al-1.2Ta-0.4Y). The Pt layer and the thermal barrier were deposited at the Surface Engineering and Nanotechnology Institute, Cranfield University.

Table 2. Details on the geometry and manufacturing process of the three batches of thermal barrier coating (TBC) systems. 't' represents the thickness, 'r' the curvature radius of the edges.

Manufacturing Process	Batch 1	Batch 2	Batch 3
Sample geometry			
Thermal Barrier (YSZ)	EB-PVD (110–120 µm) By Praxair ST	EB-PVD (150–200 µm) By Ceramic Coating Center	EB-PVD (60–80 µm) At Cranfield University
Surface preparation	By Praxair ST	Grit blasting By Safran Aircraft Engines	Grit blasting At Cranfield University
Heat Treatment	6 h at 1080 °C under high vacuum		
Pt modification	With/without electroplated Pt (7 µm ± 2 µm) By Praxair ST	Electroplated Pt (7 µm ± 2 µm) By Praxair ST	Sputtered Pt (7 µm ± 1 µm) At Cranfield University
Surface preparation	-	Smoothening	Light grinding
NiCoCrAlYTa	Tribomet® process (70–80 µm) By Praxair ST		VPS with AMDRY 997 (70–80 µm) By LERMPS
Substrate	AM3	AM3/MCNG	AM3/CMSX-4
Coated surface	Both sides		One side
TBC systems			

AM3-Trib   AM3-Trib-Pt/1   AM3-Trib-Pt/2   MCNG-Trib-Pt/2   AM3-VPS-Pt   CMSX-4-VPS-Pt

Between batches 1 and 2, the grit blasting before EB-PVD and the thermal barrier coating deposition were not made by the same companies. However, the main difference was the addition of a smoothing step on the NiCoCrAlYTa surface before Pt deposition for batch 2. To reduce the high coating roughness resulting from the VPS process, the NiCoCrAlYTa coating from batch 3 was slightly ground using P1200 SiC abrasive discs. Grinding was stopped when the proportion of ground surface, estimated by image analysis on optical microscopy images, was close to that of a partially machined surface (≈24–34% of the entire surface) [33].

In what follows, the TBC systems are named: AM3-Trib, AM3-Trib-Pt/1, AM3-Trib-Pt/2, MCNG-Trib-Pt/2, AM3-VPS-Pt, and CMSX-4-VPS-Pt (Table 2). One sample per system was tested for batches 1 and 2 (AM3-Trib, AM3-Trib-Pt/1, AM3-Trib-Pt/2, MCNG-Trib-Pt/2) while thermal cycling was performed on two samples for each system of batch 3 (AM3-VPS-Pt and CMSX-4-VPS-Pt).

2.2. Oxidation Test

Thermal cycling tests under laboratory air were carried out on the TBC systems using a vertical cyclic oxidation rig (CIRIMAT, Toulouse, France). A cycle was composed of a 1 h dwell at 1100 °C (including fast heating) and a cooling of 15 min to ambient temperature. The fast cooling rate was obtained with a high flow of air, cleaned from oil and pollution, directed towards the samples from the four sides of the sample holder. Drilled plates, maintained on a ceramic rod, were used to position the specimens. Thanks to their holes, AM3-Trib and AM3-Trib-Pt/1 TBC systems were hung to the plates using Pt wires. Samples from batches 2 and 3 were placed on a sample-holder made of a porous ceramic brick, itself placed on a plate (AM3-Trib-Pt/2, MCNG-Trib-Pt/2, AM3-VPS-Pt, and CMSX-4-VPS-Pt TBC systems). The geometry of the sample-holder was such that the thermal barrier coated surfaces were well exposed to the air flow for cooling. Samples were removed from the furnace either when spallation spread across at least 25% of the thermal barrier coated surface (AM3-Trib, AM3-Trib-Pt/1, AM3-VPS-Pt, and CMSX-4-VPS-Pt TBC systems) or at a given number of cycles (AM3-Trib-Pt/2 and MCNG-Trib-Pt/2 TBC systems). The estimate of the percentage of spalled area was done visually.

In the discussion section, thermal cycling results are compared to isothermal oxidations performed on AM3-Trib-Pt/2 and MCNG-Trib-Pt/2 TBC systems. Details on these oxidation tests can be found in [23].

2.3. Characterization

Observations by scanning electron microscopy (SEM) of sample surfaces and polished cross-sections, using the secondary electron imaging mode (SE) or the backscattered imaging mode (BSE), were done using an LEO 435VP microscope (ZEISS, Cambridge, UK). Energy-dispersive X-ray spectroscopy (EDS) analysis was performed using a PGT IMIX-PC system (Princeton Gama Tech, Princeton, USA), with real standards for quantification. Some observations of the bond-coating surface were also made using a JEOL JSM 6700F (JEOL, Japan), using the SE mode. X-ray diffraction (XRD) analyses were done using a Seifert 3000TT apparatus (Rich Seifert and Co, Ahrensburg, Germany) with a copper anti-cathode (λ = 1.54056 Å) and a grazing incidence of 4° (steps: 0.04°, time per step: 6 s).

The lifetimes of AM3-Trib, AM3-Trib-Pt/1, AM3-VPS-Pt, and CMSX-4-VPS-Pt TBC systems have already been published [31]. The present study details the microstructural characterization of the systems after thermal cycling and proposes degradation mechanisms.

3. Results

3.1. As-Processed Bond-Coatings and TBC Systems

An important characterization work on the effect of Pt on the microstructure of NiCoCrAlYTa coatings was made and discussed in a previous article [32], based on AM3-Trib-Pt/2 and AM3-VPS-Pt systems, as well as the AM3-Trib system from a batch different to the one of the present study. This previous work, combining XRD analyses, SEM observations, EDS analyses, and transmission

electron microscopy, highlighted martensite formation and Al uphill diffusion with Pt addition. Indeed, while the Trib coating, on AM3 superalloy, contained nearly 19 at % in its upper part, the AM3-Trib-Pt/2 system exhibited more than 20 at % of Al below the surface, with a peak at 24 at %. Concerning the AM3-VPS-Pt system, an Al concentration between 31 and 34 at % was measured below the surface. This section summarizes the main results of this characterization work.

At ambient temperature, the Trib coating was mainly composed of a β-NiAl phase within a γ-Ni matrix [32,34,35]. In addition, the coating exhibited a few oxide precipitates and numerous Ta carbide (TaC) precipitates [32]. Close to the superalloy, TaC carbides also contained Ti, as this element diffused fast from the superalloy towards the bond-coating surface during high temperature exposures.

At ambient temperature, the Trib-Pt/2 bond-coating consisted of an outer part, rich in Pt, composed of $L1_0$-NiAl martensite, γ'-Ni_3Al, and γ-Ni, and an inner part made of γ-Ni, containing little Pt [32]. TaC precipitates were also present close to the interface with the superalloy and many oxide particles were dispersed in the inner zone of the coating. Small oxides were also located at the position of the original Pt/NiCoCrAlYTa interface. The oxide quantity was higher for AM3-Trib-Pt/2 and MCNG-Trib-Pt/2 TBC systems compared to AM3-Trib-Pt/1 TBC system, manufactured earlier. Pores were also observed on the as-processed surface of the bond-coating of AM3-Trib-Pt/2 and MCNG-Trib-Pt/2 TBC systems, after heat treatment under vacuum (Figure 1a,b). These open pores are referred to as wells in the following.

At ambient temperature, a VPS NiCoCrAlYTa coating is composed of the β-NiAl, γ'-Ni_3Al, γ-Ni phases, and TaC uniformly dispersed throughout the coating thickness [36–38]. The addition of Pt disrupted the homogeneous microstructure [32]. The outer part of the coating was composed of a Pt-rich martensite ($L1_0$) layer over a γ'-Ni_3Al layer (a few γ'-Ni_3Al grains were also observed within the martensite layer). The inner part of the coating was Pt-rich γ-Ni/γ'-Ni_3Al, with the γ-Ni phase being the matrix. As for the Trib-Pt/2 coating, small oxides were located at the initial position of the Pt/NiCoCrAlYTa interface and open pores were visible on the bond-coating surface after the heat treatment under vacuum. However, no oxides were dispersed in the inner zone.
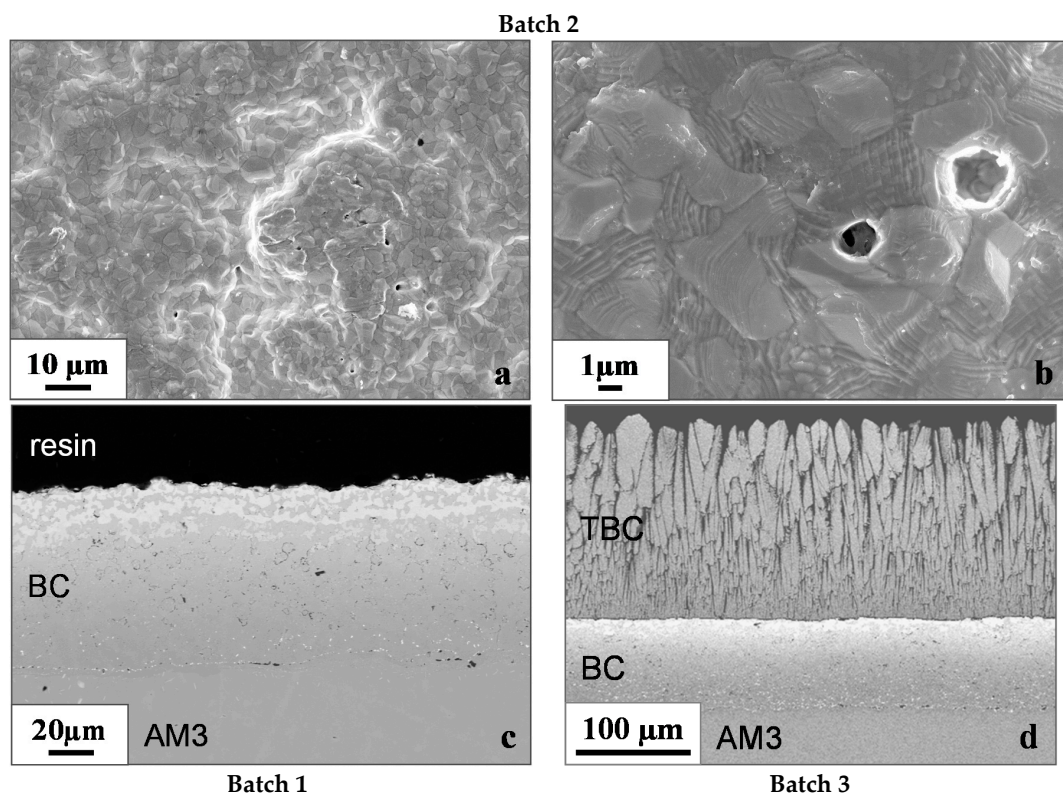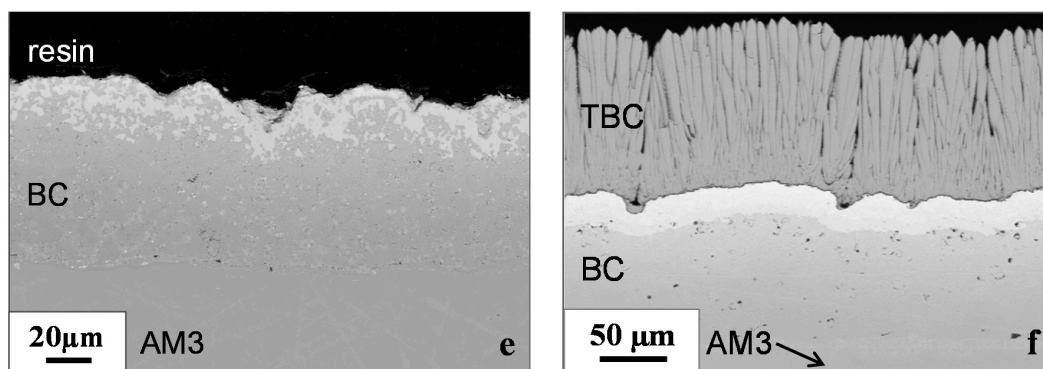
Batch 2

Batch 1   **Batch 3**

Figure 1. *Cont.*

Figure 1. (**a**,**b**) As-processed surface of the Trib-Pt/2 coating on AM3 after heat treatment under vacuum. Cross-sections of as-processed; (**c**) Trib-Pt/2 coating; and (**d**) corresponding thermal barrier coating (TBC) system on AM3; (**e**) Cross-sections of as-processed Trib-Pt/1 coating on AM3; (**f**) Cross-section of AM3-VPS-Pt TBC system. SEM images in BSE mode.

The decrease in roughness resulting from the smoothing step added in the fabrication process of the Trib-Pt/2 coating is presented in Figure 1c,e. The influence of the NiCoCrAlYTa deposition process (Tribomet® or VPS) is illustrated in Figure 1d,f. The surface of the Trib-Pt/2 coating was smooth while the surface of the VPS-Pt coating exhibited many convex and concave areas. In concave areas, the YSZ columns were tilted in relation to the general column orientation.

## 3.2. Influence of Pt on the Cyclic Oxidation Resistance of TBC Systems

Figure 2a gives the lifetimes at 1100 °C of the AM3-Trib and AM3-Trib-Pt/1 TBC systems. Because each cycle lasted 75 min and the cyclic oxidation tests were performed 24 h a day and 7 days a week, it was not possible to check the samples after each cycle. The hatched area in Figure 2a represents the lifetime uncertainty.

Cross-sections of failed AM3-Trib and AM3-Trib-Pt/1 TBC systems were observed by SEM (Figure 3). While cracking occurred at the TGO/TBC interface with the Trib bond-coating, the thermal barrier was still adherent to the TGO when Pt was added, except in concave areas where debonding occurred in the YSZ (Figure 3a–c). The surface of the Trib-Pt/1 coating was undulated and numerous conical defects were visible in the TBC, in concave areas, Figure 3a,c. Such defects, called 'corn kernel' by Birks et al. [39] or 'pinch-off' by Mumm et al. [40], were also observed in a previous study [41] after thermal cycling of TBC systems composed of a VPS NiCoCrAlYTa bond-coating. According to EDS analyses, the TGO formed on the Trib coating was mainly composed of Al_2O_3 but also contained other oxides (including Y-Al-rich oxides), Figure 3d. On the contrary, only Al_2O_3 could be detected in the oxide layer that developed on the Trib-Pt/1 coating, Figure 3e.

Because of Al consumption by oxidation, the β-NiAl phase of the Trib coating vanished, leading to a single-phased γ-Ni layer of at least 20 μm after only 36 cycles, Figure 3b. Also, the number of Ta carbides (white precipitates on BSE SEM pictures) dropped compared to the as-received coating and were mainly localized close to the superalloy (in the β-NiAl-rich zone). Ta-rich particles were also visible close to and within the TGO, Figure 3b,d. Wherever they were within the coating, the Ta-rich particles contained Ti after 36 cycles. After 290 cycles, the Trib-Pt/1 coating had evolved towards a nearly completely single-phased γ-Ni microstructure, Figure 3, with a composition in at % equal to 43.6Ni-18.1Co-20.8Cr-10.0Al-3.3Pt-0.9Ta-0.9Ti-0.8W-0.9Mo-0.7Y close to the surface based on EDS analyses. The γ'-Ni_3Al phase remained in small proportions in a few regions below the surface and at the BC/superalloy interface due to interdiffusion. Wherever it was, the γ'-Ni_3Al phase contained Ti (2.4 at % below the bond-coating surface, 2.7 at % at the interface with the superalloy, based on EDS analyses). Like the Trib, only a few carbides remained along the BC/superalloy interface of the AM3-Trib-Pt/1 TBC system, Figure 3c.
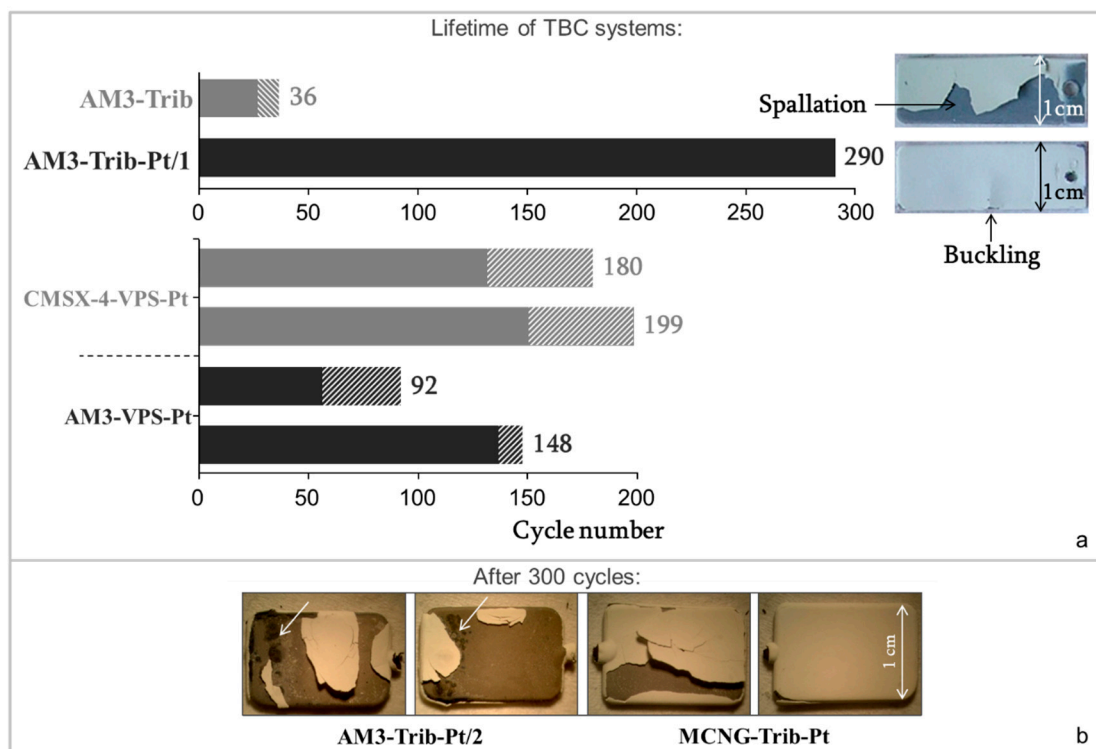
Figure 2. (**a**) Lifetime at 25% of spallation or buckling for AM3-Trib, AM3-Trib-Pt/1, AM3-VPS-Pt and CMSX-4-VPS-Pt TBC systems, and pictures of AM3-Trib and AM3-Trib-Pt/1 TBC systems after failure. The hatched areas represent the lifetime uncertainty; (**b**) Pictures of both sides of AM3-Trib-Pt/2 and MCNG-Trib-Pt/2 TBC systems after 300 cycles. The arrows indicate areas of catastrophic degradation. Thermal cycles of 1 h at 1100 °C, with a high-flow air cooling.
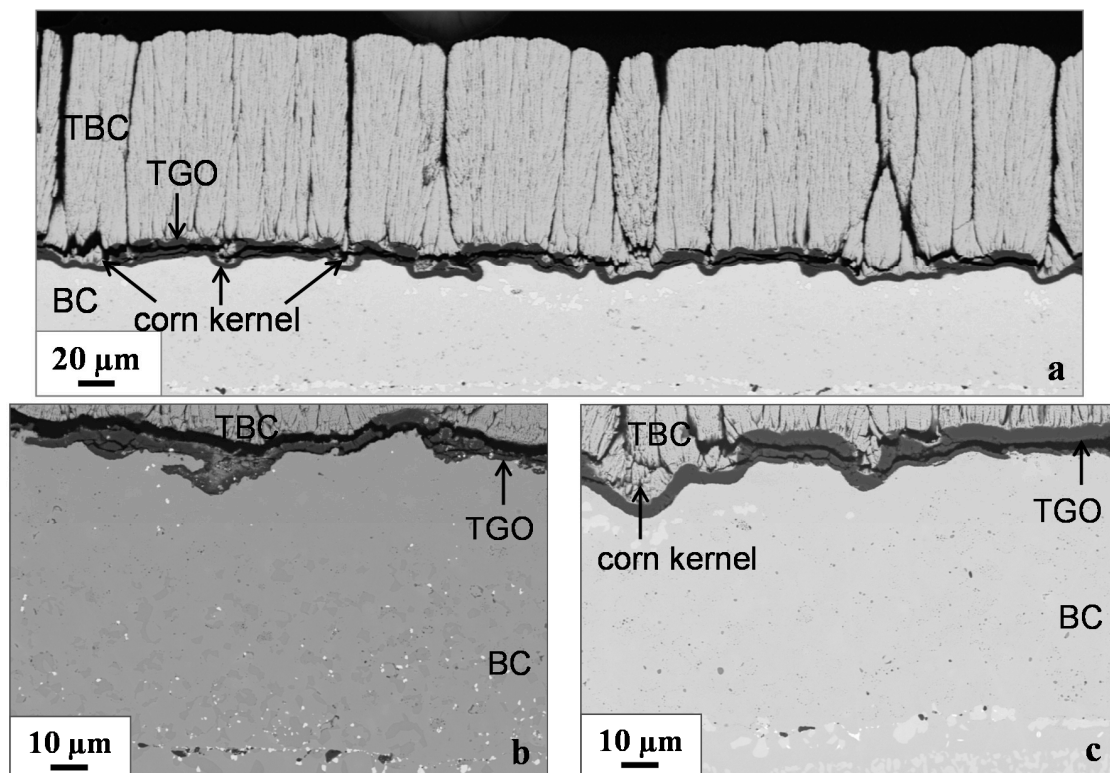

Figure 3. *Cont.*
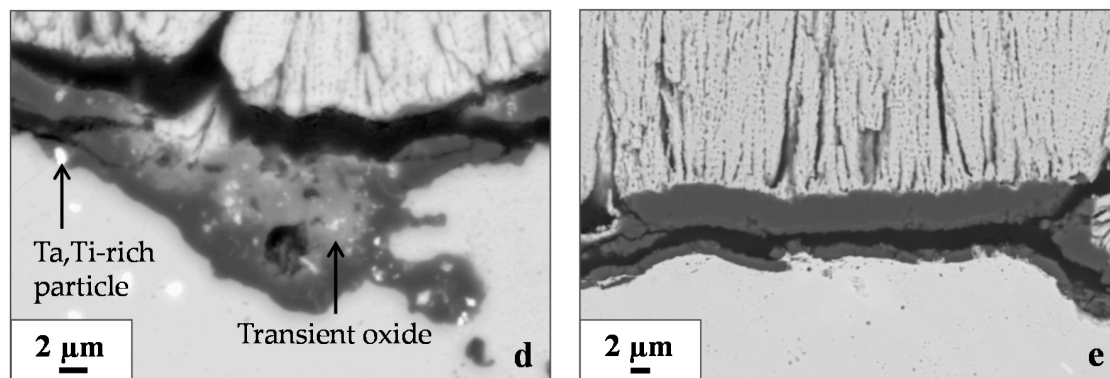
Figure 3. Cross-sections of (**a**,**c**,**e**) AM3-Trib-Pt/1 TBC system after 290 cycles; and (**b**,**d**) AM3-Trib TBC system after 36 cycles. Thermal cycles of 1 h at 1100 °C, with a high flow air cooling. (**a**) Presence of many corn kernel defects due to a rough bond-coating surface before thermal barrier deposition; (**b**) Cracking at thermally grown oxide (TGO)/thermal barrier interface; (**c**) Thermal barrier still adherent to the TGO, except at corn kernel areas; (**d**) TGO not only composed of alumina; (**e**) Only alumina detected in the TGO. SEM images in BSE mode.

### 3.3. Degradation of TBC Systems Containing a Trib-Pt/2 Coating

During the thermal cycling of TBC systems containing a Trib-Pt/2 coating, an unusual degradation was observed at one end of the AM3-base system. Therefore, this section is divided into two parts to distinguish the regular behavior of the TBC systems from the catastrophic one.

3.3.1. Healthy Area

After 300 cycles at 1100 °C, AM3-Trib-Pt/2 and MCNG-Trib-Pt/2 TBC systems exhibited spallation, Figure 2. The spalled area proportion was much larger when AM3 was the superalloy. For both systems, SEM observations on spalled areas revealed oxidized bond-coating surface with TGO flakes, Figure 4. These TGO flakes exhibited thermal barrier remains that did not look like corn kernels but rather like the broken base of YSZ columns. Oxidized wells were also visible on the bond-coating surface of the MCNG-Trib-Pt/2 TBC system, Figure 4b,c. However, cross-section observations indicated that the TGO layer was still adherent to the thermal barrier after spallation, Figure 5a,b. After 300 cycles of 1 h at 1100 °C, the bond-coating microstructure of the AM3-Trib-Pt/2 TBC system was mainly composed of the γ-Ni phase, with γ'-Ni_3Al phase regions present below the surface and at the BC/superalloy interface, Figure 5c,d. The composition, in at %, of the γ-Ni and γ'-Ni_3Al phases close to the surface were 44.4Ni-18.8Co-20.6Cr-9.2Al-4.2Pt-0.2Ta-1.0Ti-0.8W-0.9Mo and 52.4Ni-10.3Co-5.9Cr-16.2Al-7.4Pt-2.2Ta-3.2Ti-0.9W-0.7Mo-0.8Y respectively, based on EDS analyses. A few γ'-Ni_3Al regions were also observed within the internal coating zone with no TaC carbides, which was not the case for the AM3-Trib-Pt/1 TBC system after 290 cycles. For the MCNG-Trib-Pt/2 TBC system, the bond-coating was single-phased γ-Ni, with a composition in at % equal to 49.7Ni-17.3Co-16.5Cr-9.9Al-3.4Pt-0.8Ta-0.4Ti-0.9W-0.4Mo-0.3Hf-0.3Y close to the surface, based on EDS analyses. γ'-Ni_3Al regions were only visible at the BC/superalloy interface. Most carbides had disappeared and the remaining ones were localized along the interface with the superalloy.
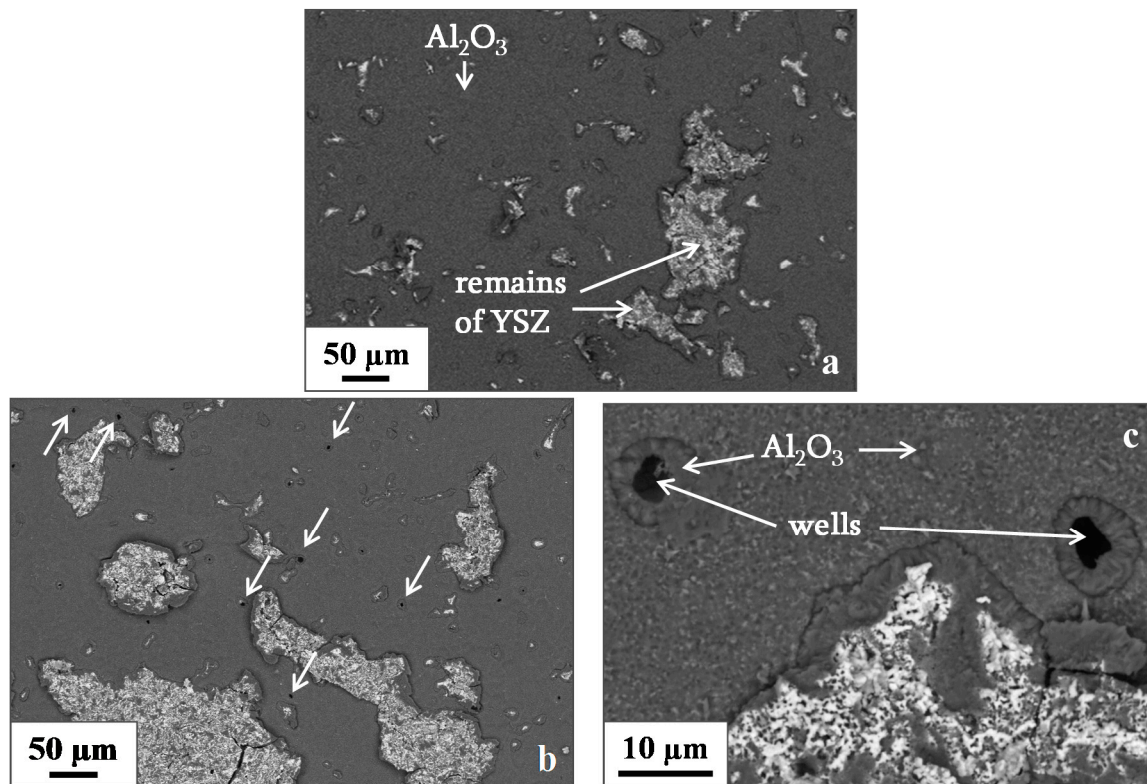
Figure 4. Bond-coating surface of (**a**) AM3-Trib-Pt/2 TBC system; (**b**,**c**) MCNG-Trib-Pt/2 TBC system after 300 cycles. The white arrows without a label identify the oxidized wells. Thermal cycles of 1 h at 1100 °C, with a high-flow air cooling. SEM images in BSE mode.
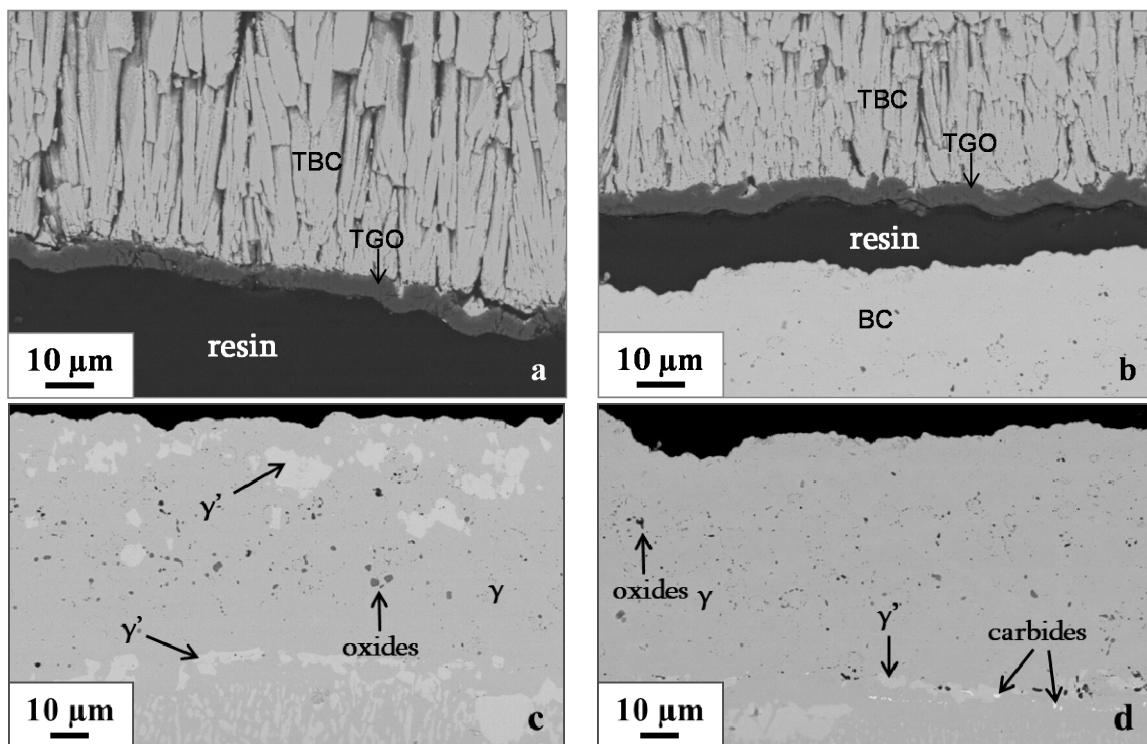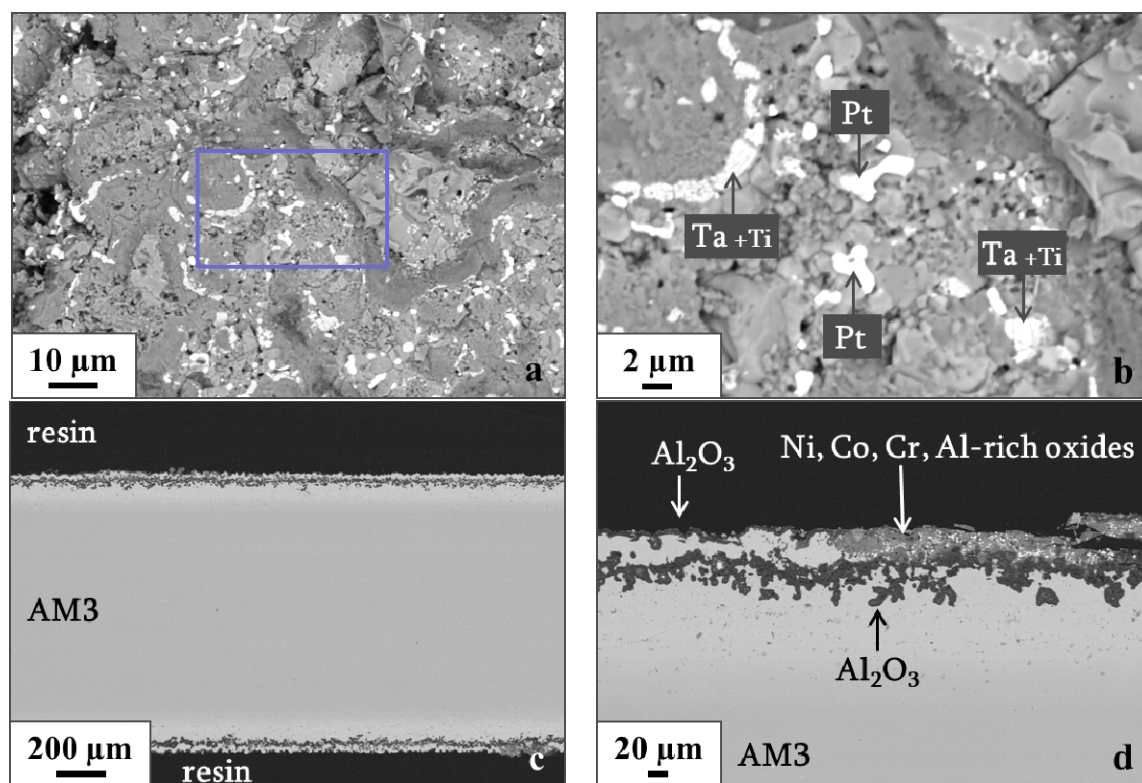

Figure 5. Cross-sections of (**a**,**c**) AM3-Trib-Pt/2 TBC system; and (**b**,**d**) MCNG-Trib-Pt/2 TBC system after 300 cycles. Thermal cycles of 1 h at 1100 °C, with a high-flow air cooling. SEM images in BSE mode.
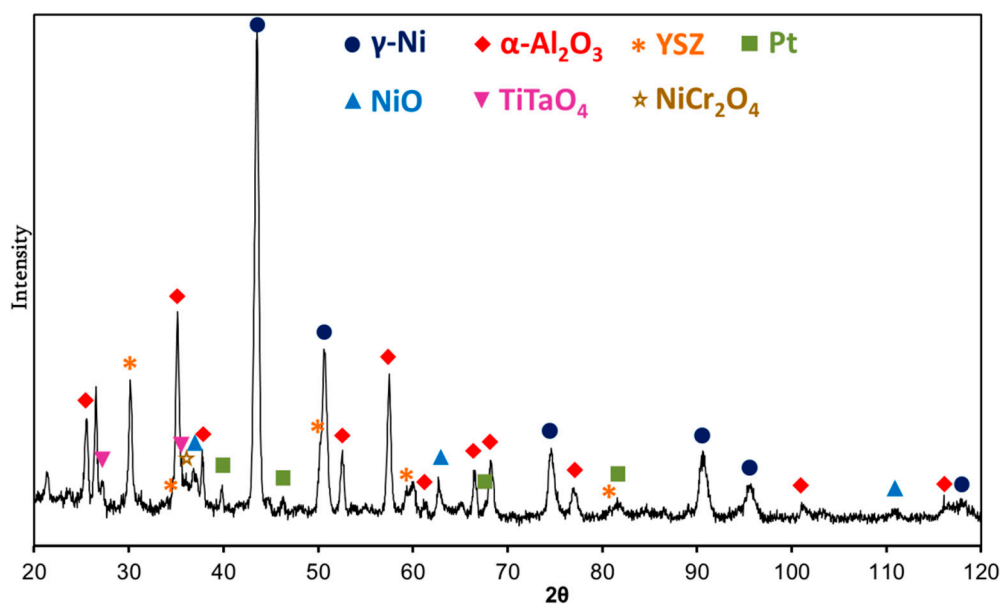
3.3.2. Area of Catastrophic Degradation

After only 300 cycles, an unusual degradation was observed on the bond-coating surface of the AM3-Trib-Pt/2 TBC system, as pointed out by the arrows on Figure 2b,c. Next, SEM observations of the bond-coating surface and cross-section were done on this specific area, Figure 6. On the surface, particles, either Pt-rich or Ta-rich (containing also some Ti for the latter), were dispersed in (Ni, Co, Cr, Al)-rich oxides. An XRD analysis done on this specific area confirmed the presence of other oxides than alumina (like NiO, $NiCr_2O_4$, and $TiTaO_4$) and revealed that the Pt-rich particles were pure Pt, Figure 7. Cross-section observations showed that this unusual degradation concerned the entire circumference of one sample end, Figure 6c. (Ni, Co, Cr, Al)-rich oxides containing Pt and Ta-rich particles did not spread over the entire surface, Figure 6d, while an Al_2O_3 layer dividing the bond-coating into two zones, an outer zone and an inner one, was present along the entire sample circumference, Figure 6c. No Al was detected by EDS in the region situated between the external oxide scale and the inner Al_2O_3 layer. Such catastrophic degradation was not observed for the MCNG-Trib-Pt/2 TBC system despite oxide penetrating within the bond-coating in a few areas, Figure 8.

Figure 6. Area of catastrophic degradation of AM3-Trib-Pt/2 TBC system, after 300 cycles; (**a**,**b**) Surface morphology of the bond-coating, (**b**) is an enlargement of the rectangle area of (**a**) showing Ta-rich particles (containing some Ti) and Pt-particles; (**c**,**d**) Cross-sections (**c**) showing the extent of the catastrophic degradation and (**d**) giving details on the degraded area exhibiting external (Ni, Co, Cr, Al)-rich oxides and internal alumina. Thermal cycles of 1 h at 1100 °C, with a high-flow air cooling. SEM images in BSE mode.

Figure 7. X-ray diffraction (XRD) diagram obtained from the bond-coating surface of the AM3-Trib-Pt/2 TBC system, in the area of catastrophic degradation.
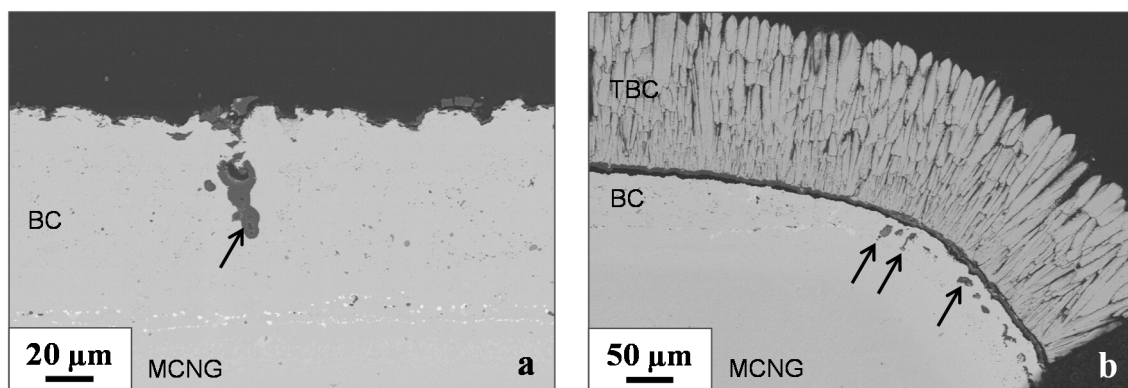

Figure 8. Cross-sections of the MCNG-Trib-Pt/2 TBC system after 300 cycles. The arrows identify zones of oxide penetration within the bond-coating, (**a**) on one sample face, (**b**) on one sample corner. Thermal cycles of 1 h at 1100 °C, with a high-flow air cooling. SEM images in BSE mode.

3.4. Degradation of TBC Systems with a VPS-Pt Bond-Coating

The lifetimes of AM3-VPS-Pt and CMSX-4-VPS-Pt TBC systems are presented in Figure 2. The average lifetime of the AM3-base systems was shorter than the average lifetime of the CMSX-4-base systems.

After thermal cycling, bond-coating surfaces and cross-sections were observed by SEM, Figure 9. The features are shown for the AM3-VPS-Pt TBC system that lasted 92 cycles but they were identical whatever the superalloy. First, many corn kernels were visible on the bond-coating surface after spallation, Figure 9a,b,d. Second, the oxide scale was an almost exclusive Al_2O_3 layer but contained Ti, according to EDS analyses, and it exhibited cavities, Figure 9b. The bond-coating surface was deformed, Figure 9b–d, and some oxide penetrations within the bond-coating were visible, as for the CMSX-4-VPS-Pt TBC system that lasted 199 cycles, Figure 9d. The bond-coating was no longer composed of the martensitic phase, Figure 9c,d. A thick discontinuous γ'-Ni_3Al layer, Ti-and Ta-rich, was present close to the surface and in the interdiffusion zone. The composition of this γ'-Ni_3Al layer was, in at %, equal to 49.2Ni-11.3Co-6.1Cr-17.9Al-8.1Pt-3.5Ta-1.8Ti-0.9W-0.5Mo-0.7Y and 49.7Ni-11.7Co-5.4Cr-16.4Al-8.4Pt-4.2Ta-1.2Ti-1.2W-0.1Mo-0.2Re-0.3Hf-1.2Y for AM3-base and

CMSX-4-base systems respectively, based on EDS analyses. The inner part of the coating was composed of γ-Ni. A few isolated γ'-Ni$_3$Al grains were also visible within the inner part, below the discontinuous γ'-Ni$_3$Al layer, as few isolated γ-Ni grains were present above the thick γ'-Ni$_3$Al layer.
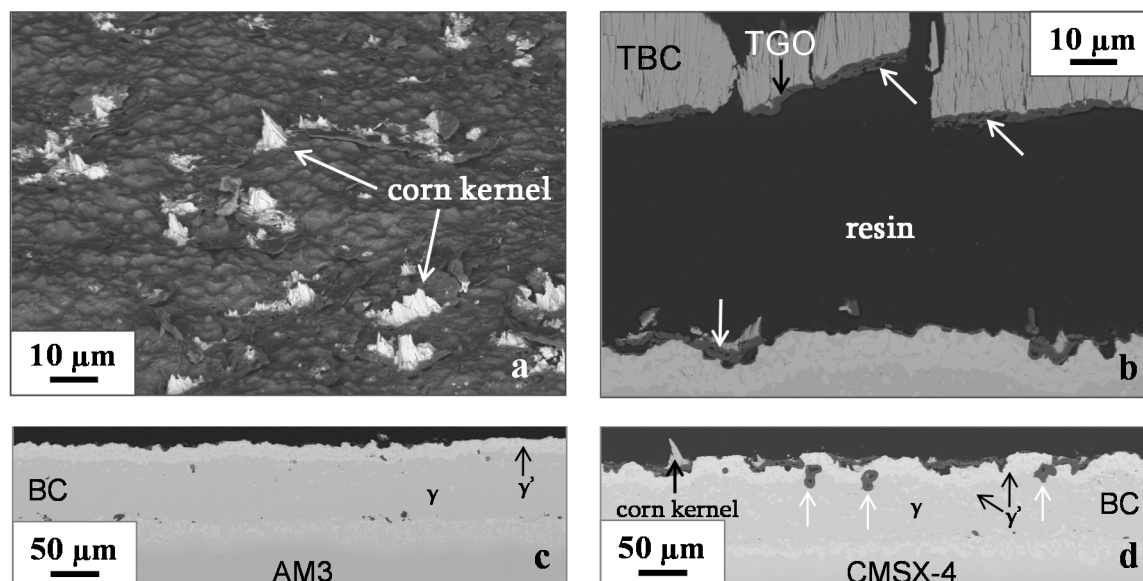
Figure 9. (**a**) Tilted VPS-Pt coating surface after spallation; (**b**,**c**) Cross-sections of the AM3-VPS-Pt TBC system after 92 cycles; (**d**) Cross-section of the CMSX-4-VPS-Pt TBC system after 199 cycles. The white arrows identify (**a**) the cavities within the TGO and (**c**) the oxide that locally penetrated deep within the bond-coating. Thermal cycles of 1 h at 1100 °C, with a high-flow air cooling. SEM images in BSE mode.

4. Discussion

4.1. Pt Effect on the Cyclic Oxidation Resistance of TBC Systems with a Trib Bond-Coating

AM3-Trib and AM3-Trib-Pt/1 TBC systems were thermally cycled at 1100 °C (batch 1). A large increase in lifetime was obtained with Pt addition (from 36 to 290 cycles). Even though only one sample per system was tested, this confirms the beneficial effect of Pt on the oxidation resistance of TBC systems. However, 290 cycles is a short lifetime for turbine blade applications, even for a system based on a 1st generation superalloy. Therefore, it is necessary to understand the reasons for these short lifetimes.

For the AM3-Trib TBC system, crack propagation occurred at the TGO/TBC interface and the TGO layer was mainly composed of Al$_2$O$_3$, but contained other oxides. The presence of oxides other than Al$_2$O$_3$ on top of the TGO was responsible for the weak adherence of the thermal barrier to the TGO layer and explains the very short lifetime of the system. Y-Al-rich oxides and Ta-Ti-rich particles were also present on the TGO layer. During bond-coating oxidation, oxides of reactive elements, such as Hf or Y, can form and lead to peg formation. Pegs act as mechanical anchorage points and favor the TGO adherence to the bond-coating [42–46]. However, peg formation leads to local deformations of the BC/TGO interface, an increase in TGO thickness, and heterogeneities in TGO composition that result in stress concentrations during thermal cycling. Therefore, a high peg density causes a shorter lifetime [17,47–50]. The presence of Y-Al-rich oxides within the TGO after only 36 cycles suggests that the Y content of the bond-coating is too high. Concerning Ti, most authors agree that it is harmful with regard to oxidation [34,35,51–56]. One way to reduce its detrimental effect on oxidation consists in adding Ta to the NiCoCrAlY because Ta traps Ti and C diffusing from the superalloy towards the oxide scale by forming (Ta, Ti) C carbides [9,18,57,58]. Therefore, Ta decreases the superalloy effect on the oxidation behavior [34] since Ti can no longer diffuse towards the TGO. Regarding the AM3-Trib-Pt/1 system, the TBC was still adherent to the TGO after 290 cycles and only Al$_2$O$_3$ could be detected in the

oxide scale. This last observation confirms that Pt favors Al selective oxidation, as demonstrated in one of our previous studies [23] and as already observed by others [19,20]. This is explained by the decrease in Al activity due to the presence of Pt, as shown by others [59,60], which led to an Al-uphill diffusion during the vacuum heat treatment. The AM3-Trib-Pt/1 TBC system failure was not due to heterogeneity of the TGO in terms of composition and thickness. Rather it was due to the presence of numerous corn kernel defects, characteristic of a surface exhibiting concave areas before thermal barrier deposition by EB-PVD. When the TGO/TBC interface is strong, the thermal barrier prevents the development of bond-coating surface undulations [20,61–63]. Because corn kernel defects are lightly bonded to the thermal barrier coating, the bond-coating surface deformation is easier in these specific areas. Furthermore, TGO undulations in the corn kernel areas lead to stress concentration and to fracture, according to Evans et al. [5]. In the present study, the presence of many corn kernels shows that the Pt electroplating process did not smooth the rough NiCoCrAlYTa bond-coating surface.

By forming an exclusive Al_2O_3 layer, the Trib-Pt coating was closer to Pt-modified nickel aluminide coating whose degradation is mainly due to rumpling. Various explanations have been given for rumpling development, among them the martensite transformation of β-NiAl [64] coupled with coating creep [65]. With an outer zone rich in martensite, the Trib-Pt coating is more affected by rumpling than the NiCoCrAlYTa. This could constitute a drawback for such a coating, but this needs to be confirmed for longer lifetimes. Indeed, this may depend on the duration of the martensite presence below the oxide scale.

4.2. Failure Mechanism of AM3-Trib-Pt/2 and MCNG-Trib-Pt/2 TBC Systems

SEM observations of the Trib-Pt/2 bond-coatings after 300 cycles revealed that spalled areas were oxidized (Figure 4) while the TGO layer was still adherent to the thermal barrier (Figure 5a,b). As spallation occurred before 300 cycles, cracking probably happened along the BC/TGO interface and cycling continuation led to the bond-coating surface oxidation under the detached TGO. For these TBC systems, an additional surface preparation step was added to smooth the Trib coating surface before Pt deposition. For both systems, no corn kernel defect was visible after spallation. This highlights the relevance of smoothing the bond-coating surface before EB-PVD in order to minimize thermal barrier defects. However, despite this additional surface preparation step, the AM3-Trib-Pt/2 TBC system lifetime was not improved when compared to the one of AM3-Trib-Pt/1 TBC system. This is likely due to the catastrophic degradation observed on the AM3-Trib-Pt/2 TBC system.

After heat treatment under vacuum, the surface of Trib-Pt/2 bond-coatings exhibited a deep open porosity, for both superalloys (AM3 and MCNG). In addition, these bond-coatings contained numerous oxides in the inner zone [23]. This may mean that oxygen was trapped during coating fabrication because of CrAlYTa particle oxidation. Thus, during heat treatment under vacuum, oxides could limit interdiffusion between the CrAlYTa particles and the (Ni, Co) matrix, leading to oxidized and not very dense areas (at the former CrAlYTa/(Ni, Co) interfaces) and therefore creating a porosity network. This porosity network and the wells play a major role in the proposed failure mechanism, Figure 10. During the thermal cycling test under laboratory air, the bond-coating surface (including the planar areas and the wells) oxidized to form an Al_2O_3 layer. The volume expansion (due to the formation of intergranular Al_2O_3) added to the large thermal stresses generated during the rapid coolings and heatings of the thermal cycling test (due to coefficient of thermal expansion mismatch [5]), favored bond-coating micro-cracking at the well points. Because of micro-cracking, the oxide progressively penetrated within the bond-coating during cycling. When the oxide layer developed in these wells reached the former CrAlYTa/(Ni, Co) interfaces, its propagation parallel to the coating surface was favored by the oxides already there. Its propagation was also mainly favored by the lack of coating cohesion at these particular zones. Finally, intergranular oxidation progressed along this porosity network within the bond-coating. As Al was consumed at the surface but also at the wells and at the CrAlYTa/(Ni, Co) interfaces, it was no longer available to ensure the growth of an external protective Al_2O_3 scale. This was made even worse by the Al_2O_3 that developed internally, parallel to

the bond-coating surface, blocking the Al up-hill diffusion towards the external surface. When the Al content and the Al flux below the TGO became inferior to the critical values required for Al_2O_3 formation, other oxides formed. These oxides, rich in Ni, Co, Cr, and Al, developed during this breakaway oxidation stage and led to the system failure. This proposed degradation mechanism is therefore a mix between the Intrinsic Chemical Failure and the Mechanically Induced Failure [66].
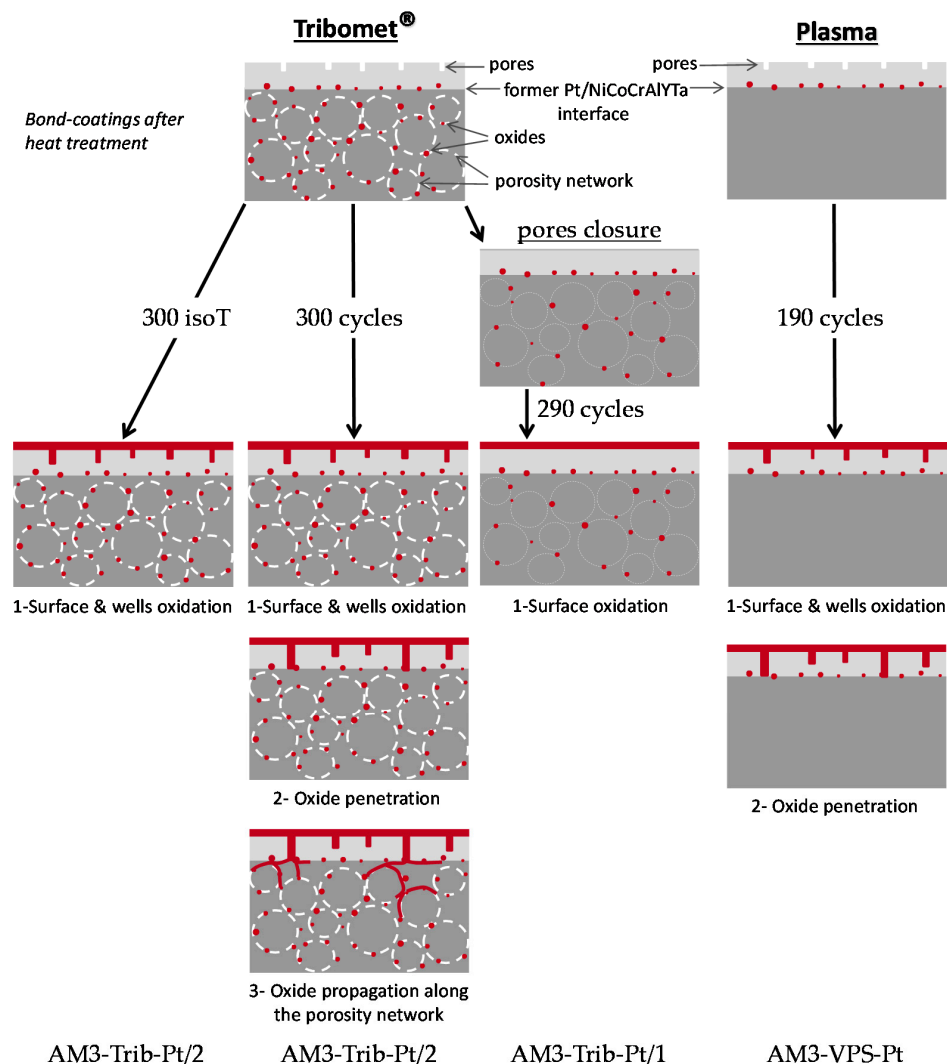
Figure 10. Proposed degradation mechanisms for TBC systems composed of a Pt-modified NiCoCrAlYTa bond-coating.

Although the MCNG-Trib-Pt/2 and the AM3-Trib-Pt/2 TBC systems were fabricated at the same time and tested for the same number of cycles, the MCNG-base TBC system did not exhibit catastrophic degradation. Sulfur, contained in the superalloys, is well-known for its detrimental effect on TGO adherence [67–72]. In the present study, the difference in lifetime is unlikely to be due to the sulfur content of the superalloy as both superalloys contained less than 0.5 ppmw (concentrations determined by glow discharge mass spectroscopy, GDMS). The only known differences are the Pt quantity [32] and the oxidation rate constant [23] of the coating as well as the superalloy Ti content, all higher for the AM3-base system, and the Hf doping of MCNG superalloy. A greater Pt content is generally thought to be beneficial. Nevertheless, a higher Pt quantity led to a larger martensite quantity in the external layer, as observed on cross-sections. As mentioned previously, the martensitic transformation is known to favor rumpling apparition in nickel aluminide coatings. The presence of martensite may well favor propagation within the bond-coating and therefore catastrophic degradation. Also, a higher oxidation

rate and the absence of Hf in the AM3-Trib-Pt/2 TBC system could have led to larger stresses within the wells and easier metal/Al_2O_3 interfacial crack propagation.

Even if no catastrophic degradation was observed for the MCNG-Trib-Pt/2 TBC system, oxidation penetration was encountered locally. This appeared similar to the onset of the catastrophic degradation that started on the edge for the AM3-Trib-Pt/2 TBC system. The higher surface/volume ratio at edges and corners explains the faster consumption of the Al reservoir contained within the material. Thermo-mechanical stresses are also higher and the quality of surface preparation is lower in these regions. All these reasons explain why degradation is greater at the sample edges. An increase in degradation in areas with a low curvature radius has previously been observed [73–75].

Catastrophic degradation occurred for the AM3-Trib-Pt/2 TBC system after 300 cycles at 1100 °C while this was not encountered for the AM3-Trib-Pt/1 TBC system that lasted 290 cycles at the same temperature. As explained previously, these TBC systems were not fabricated at the same time. The AM3-Trib-Pt/1 TBC system had a hole and a bond-coating over-thickness, while the AM3-Trib-Pt/2 TBC system had a welded stem. The thermal barrier thickness also differed between these batches. Due to these differences, the TBC system lifetimes must be compared with caution. Although the inner part of the Trib-Pt/1 bond-coating contained oxides, the oxide quantity was much lower than the one of the Trib-Pt/2 bond-coating. This prevented catastrophic degradation for the AM3-Trib-Pt/1 TBC system. Such an issue has already been mentioned by Subanovic et al. [76]. In their study, they showed that when the oxygen partial pressure within the VPS chamber was high enough, oxides rich in reactive elements were present through VPS NiCoCrAl(Y/Hf) coatings that exhibited poor oxidation behavior. Two other differences between these systems have to be mentioned: the surface preparation before Pt electroplating and before thermal barrier deposition. While for the AM3-Trib-Pt/1 TBC systems the bond-coating surface preparation was made at Praxair ST (the Tribomet® NiCoCrAlYTa coating manufacturer, Oldmixon, UK), the bond-coating surface of the AM3-Trib-Pt/2 TBC system was grit-blasted at Safran Aircraft Engines (Châtellerault, France), according to parameters optimized for Pt-modified nickel aluminide coatings. It is then possible that the grit blasting carried out at Safran Aircraft Engines was insufficient to close the wells present at the Trib-Pt/2 surface. On the contrary, a surface preparation suitable for Trib coatings closed this open porosity and therefore prevented catastrophic degradation, Figure 10.

Finally, when the AM3-Trib-Pt/2 TBC system was oxidized isothermally [23], no thermal stress developed. Therefore, no micro-crack formed, oxide did not penetrate through the bond-coating depth, and no catastrophic degradation was observed.

4.3. Failure Mechanism of TBC Systems with a VPS-Pt Bond-Coating

Despite a significant difference in lifetime between AM3-VPS-Pt and CMSX-4-VPS-Pt TBC systems, the uncertainty domains had to be taken into account. The lifetimes of both TBC systems tend to be different, but additional data would be necessary to confirm. Nevertheless, from the present data, it is reasonable to say that the superalloy may influence the cyclic oxidation behavior of TBC systems with a VPS-Pt coating.

The S content of AM3 and CMSX-4 superalloys was measured by GDMS; 0.28 ppmw in AM3 against 1.4 ppmw in CMSX-4. The higher S content should have accelerated the degradation of the CMSX-4-VPS-Pt TBC systems but thermal barrier spallation occurred more rapidly with AM3 superalloy. Hf, contained in CMSX-4, is a reactive element known to mitigate the detrimental effect of S [67,77–79]. Therefore, the presence of Hf compensated the higher S content of CMSX-4 and the difference in TBC system lifetime could not be explained by the difference of S concentration. In a previous study, a Trib-Pt/2 coating deposited on MCNG, Hf-rich, exhibited a slightly lower oxidation rate than the same coating on AM3, which is Hf-free [23]. Thus, the presence of Hf in CMSX-4 and its possible effects on the oxidation rate and oxide scale adherence could have been beneficial for the TBC system lifetime. However, further analyses are necessary to understand why the CMSX-4-based TBC system had a better behavior.

In both systems, only Al_2O_3 could be detected in the oxide scale that also contained some Ti, as shown in [31]. This confirms the beneficial effect of Pt on Al-selective oxidation and the rapid Ti diffusion from the superalloy toward the oxide scale. Cavities were also observed within the TGO, which was not the case for the TBC systems with a Trib-Pt coating. Parameters used during Pt deposition by sputtering influence the microstructure and the degradation of Pt-modified nickel aluminide coatings. Non optimized sputtering parameters could lead to cavities within the TGO [80].

Numerous corn kernel defects were visible at the bond-coating surface after spallation, proof that the bond-coating surface was too rough before EB-PVD. It can be concluded that the light grinding made after VPS did not lead to a surface finish suitable for EB-PVD. However, a complete grinding of the VPS NiCoCrAlYTa was not recommended before sputtering a 7 μm Pt layer since thick layers may come off from a smooth substrate during deposition or may generate cavities during diffusion heat treatment.

After vacuum heat treatment, deep concave zones were visible at the surface of VPS-Pt coatings. After thermal cycling, their surface was greatly deformed and at some regions oxide penetrated within the bond-coating and could even reach the original Pt/NiCoCrAlYTa interface. Like for the cavities present within the TGO, the large bond-coating deformation could be due to the sputtering process. It could also be due to the martensitic transformation of β-NiAl. Complementary tests would be necessary to better understand this.

Despite deep oxide penetration, up to the former Pt/NiCoCrAlYTa interface, oxidation did not propagate parallel to the bond-coating surface. This can be explained by a lower number of cycles but it may also be due to the absence of oxide and porosity in the inner zone of VPS bond-coatings after fabrication. Even if the oxidized wells penetrated deep inside the bond-coating during thermal cycling, they could not follow any porosity network and therefore did not propagate parallel to the surface, Figure 10.

It is interesting to point out that Jackson et al. [22] noticed deep oxide protrusions in NiCoCrAlY coatings deposited by argon-shrouded plasma spraying after 2067 cycles at 1100 °C (cycles with a 45 min hot dwell). This was observed only in the case of high Y-content coatings (0.5 wt % versus 0.1 wt %) with a rough surface. They proposed that the protrusions were initiated by preferential oxidation of Y in concave regions of the coating surface. They did not claim any mechanism relative to the protrusion propagation due to a lack of data, but mentioned the possibility of cracking.

5. Conclusions

In this study, many TBC systems that differ by fabrication process (Pt addition, deposition techniques, surface preparation steps) were oxidized. The results confirm that Pt is beneficial in terms of TBC system lifetime under thermal cycling conditions as it favors Al selective oxidation on a Trib coating, by martensitic (Ni, Pt) Al formation. On the other hand, Pt seems to destabilize TaC carbides that trap Ti. The beneficial effect of Pt on the cyclic oxidation resistance of Trib-base TBC systems is then mitigated when used in systems based on Ti-rich superalloys. Moreover, martensite formation led to stress development in the coating.

While the short lifetime of AM3-Trib-Pt/1 TBC systems was attributed to numerous corn kernel defects because of a rough bond-coating surface before EB-PVD, AM3-Trib-Pt/2 and MCNG-Trib-Pt/2, TBC systems failed because the Trib coating contained numerous oxide precipitates and was not dense enough. Concerning AM3-VPS-Pt and CMSX-VPS-Pt TBC systems their short lifetime was due to non-optimized sputtering parameters and a great density of corn kernel defects. This highlights the relevance of smoothing the NiCoCrAlYTa surface before Pt deposition to obtain, after heat treatment under vacuum, a bond-coating roughness suitable for EB-PVD.

Finally, the present work shows that the TBC system lifetime is increased when: (i) the NiCoCrAlYTa coating is dense, well-interdiffused and oxide-free; (ii) the NiCoCrAlYTa surface is smoothed before Pt deposition; and (iii) defects on the bond-coating surface are removed by a suitable surface preparation before EB-PVD.

References

1. Nicholls, J.R.; Deakin, M.J.; Rickerby, D.S. A comparison between the erosion behaviour of thermal spray and electron beam physical vapour deposition thermal barrier coatings. *Wear* **1999**, *233*, 352–361. [CrossRef]
2. Wellman, R.G.; Deakin, M.J.; Nicholls, J.R. The effect of TBC morphology and aging on the erosion rate of EB-PVD TBCs. *Wear* **2005**, *258*, 349–356. [CrossRef]
3. Mercer, C.; Faulhaber, S.; Evans, A.G.; Darolia, R. A delamination mechanism for thermal barrier coatings subject to calcium-magnesium-alumino-silicate (CMAS) infiltration. *Acta Mater.* **2005**, *53*, 1029–1039. [CrossRef]
4. Krämer, S.; Faulhaber, S.; Chambers, M.; Clarke, D.R.; Levi, C.G.; Hutchinson, J.W.; Evans, A.G. Mechanisms of cracking and delamination within thick thermal barrier systems in aero-engines subject to calcium-magnesium-alumino-silicate (CMAS) penetration. *Mater. Sci. Eng. A* **2008**, *490*, 26–35. [CrossRef]
5. Evans, A.G.; Mumm, D.R.; Hutchinson, J.W.; Meier, G.H.; Pettit, F.S. Mechanisms controlling the durability of thermal barrier coatings. *Prog. Mater Sci.* **2001**, *46*, 505–553. [CrossRef]
6. Lipkin, D.M.; Clarke, D.R.; Hollatz, M.; Bobeth, M.; Pompe, W. Stress development in alumina scales formes upon oxidation of (111) NiAl single crystals. *Corros. Sci.* **1997**, *39*, 231–242. [CrossRef]
7. Reddy, A.; Hovis, D.B.; Heuer, A.H.; Paulikas, A.P.; Veal, B.W. In Situ Study of Oxidation-Induced Growth Strains in a Model NiCrAlY Bond-Coat Alloy. *Oxid. Met.* **2007**, *67*, 153–177. [CrossRef]
8. Lipkin, D.M.; Clarke, D.R. Measurement of the Stress in Oxide Scales Formed by Oxidation of Alumina-Forming Alloys. *Oxid. Met.* **1996**, *45*, 267–280. [CrossRef]
9. Mevrel, R. State of art on High-Temperature Corrosion-resistant Coatings. *Mater. Sci. Eng. A* **1989**, *A120*, 13–24. [CrossRef]
10. Nicholls, J.R. Designing oxidation-resistant coatings. *JOM* **2000**, *52*, 28–35. [CrossRef]
11. Nicholls, J.R. Advances in coating design for high-performance gas turbines. *MRS Bull.* **2003**, *28*, 659–670. [CrossRef]
12. Pomeroy, M.J. Coatings for gas turbine materials and long term stability issues. *Mater. Des.* **2005**, *26*, 223–231. [CrossRef]
13. Eliaz, N.; Shemesh, G.; Latanision, R.M. Hot corrosion in gas turbine components. *Eng. Fail. Anal.* **2002**, *9*, 31–43. [CrossRef]
14. Whittle, D.P.; Stringer, J. Improvements in high temperature oxidation resistance by additions of reactive elements or oxide dispersions. *Philos. Trans. R. Soc. Lond.* **1980**, *A295*, 309. [CrossRef]
15. Felten, E.J. Use of Platinum and Rhodium to Improve Oxide Adherence on Ni-8Cr-6Al Alloys. *Oxid. Met.* **1976**, *10*, 23–28. [CrossRef]
16. Lowrie, R.; Boone, D.H. Composite coatings of CoCrAlY plus platinum. *Thin Solid Films* **1977**, *45*, 491–498. [CrossRef]
17. Peichl, L.; Bettridge, D.F. Overlay and diffusion coatings for aero gas turbines. In *Materials for Advanced Power Engineering, Part I*; Springer Netherlands: Dordrecht, The Netherlands, 1994.
18. Taylor, T.A.; Bettridge, D.F. Development of alloyed and dispersion-strengthened MCrAlY coatings. *Surf. Coat. Technol.* **1996**, *86–87*, 9–14. [CrossRef]
19. Quadakkers, W.J.; Shemet, V.; Sebold, D.; Anton, R.; Wessel, E.; Singheiser, L. Oxidation characteristics of a platinized MCrAlY bond coat for TBC systems during cyclic oxidation at 1000 °C. *Surf. Coat. Technol.* **2005**, *199*, 77–82. [CrossRef]

20. Yanar, N.M.; Pettit, F.S.; Meier, G.H. Failure Characteristics during Cyclic Oxidation of Yttria Stabilized Zirconia Thermal Barrier Coatings Deposited via Electron Beam Physical Vapor Deposition on Platinum Aluminide and on NiCoCrAlY Bond Coats with Processing Modifications for Improved Performances. *Metall. Mater. Trans. A* **2006**, *37A*, 1563–1580.

21. Feuerstein, A.; Knapp, J.; Taylor, T.; Ashary, A.; Bolcavage, A.; Hitchman, N. Technical and Economical Aspects of Current Thermal Barrier Coating Systems for Gas Turbine Engines by Thermal Spray and EBPVD: A Review. *J. Ther. Spray Technol.* **2008**, *17*, 199–213. [CrossRef]

22. Jackson, E.M.M.; Yanar, N.M.; Maris-Jakubowski, M.C.; Onal-Hance, K.; Meier, G.H.; Pettit, F.S. Effect of surface preparation on the durability of NiCoCrAlY coatings for oxidation protection and bond coats for thermal barrier coatings. *Mater. Corros.* **2008**, *59*, 494–500. [CrossRef]

23. Vande Put, A.; Oquab, D.; Péré, E.; Raffaitin, A.; Monceau, D. Beneficial Effect of Pt and of Pre-Oxidation on the Oxidation Behaviour of an NiCoCrAlYTa Bond-Coating for Thermal Barrier Coating Systems. *Oxid. Met.* **2011**, *75*, 247–279. [CrossRef]

24. Yanar, N.M.; Meier, G.H.; Pettit, F.S. The influence of platinum on the failure of EBPVD YSZ TBCs on NiCoCrAlY bond coats. *Scr. Mater.* **2002**, *46*, 325–330. [CrossRef]

25. Joo, D.; Park, S.-H.; Jung, Y.-G.; Lee, J.-H.; Ye, C.-H.; Lee, K.-H. Effect of Platinum Pre-Coating on Isothermal Oxidation Behavior of MCrAlY Coating by Plasma Spray Process. *Mater. Sci. Forum* **2007**, *544–545*, 721–724. [CrossRef]

26. Monceau, D.; Oquab, D.; Estournes, C.; Boidot, M.; Selezneff, S.; Thebault, Y.; Cadoret, Y. Pt-modified Ni aluminides, MCrAlY-base multilayer coatings and TBC systems fabricated by Spark Plasma Sintering for the protection of Ni-base superalloys. *Surf. Coat. Technol.* **2009**, *204*, 771–778. [CrossRef]

27. Monceau, D.; Oquab, D.; Estournes, C.; Boidot, M.; Selezneff, S.; Ratel-Ramond, N. Thermal Barrier Systems and Multi-Layered Coatings Fabricated by Spark Plasma Sintering for the Protection of Ni-Base Superalloys. *Mater. Sci. Forum* **2010**, *654–656*, 1826–1831. [CrossRef]

28. Lan, H.; Yang, Z.; Zhang, Y.; Zhang, C. Influence of Pt on Oxidation Behavior of CoNiCrAlY Alloy. *Rare Met. Mater. Eng.* **2012**, *41*, 194–198.

29. Lan, H.; Zhang, W.; Yang, Z. Investigation of Pt-Dy co-doping effects on isothermal oxidation behavior of (Co,Ni)-based alloy. *J. Rare Earths* **2012**, *30*, 928. [CrossRef]

30. Tawancy, H.M. Comparative Structure, Oxidation Resistance and Thermal Stability of CoNiCrAlY Overlay Coatings with and Without Pt and Their Performance in Thermal Barrier Coatings on a Ni-Based Superalloy. *Oxid. Met.* **2018**, *90*, 383–399. [CrossRef]

31. Vande Put, A.; Oquab, D.; Raffaitin, A.; Monceau, D. Effect of Pt addition on the cyclic oxidation resistance of NiCoCrAlYTa base TBC systems. In Proceedings of the Eurocorr Conference, Nice, France, 6–10 September 2009.

32. Vande Put, A.; Lafont, M.C.; Oquab, D.; Raffaitin, A.; Monceau, D. Effect of modification by Pt and manufacturing processes on the microstructure of two NiCoCrAlYTa bond coatings intended for thermal barrier system applications. *Surf. Coat. Technol.* **2010**, *205*, 717–727. [CrossRef]

33. Monceau, D.; Crabos, F.; Malie, A.; Pieraggi, B. Effects of bond-coat preoxidation and surface finish on isothermal and cyclic oxidation, high temperature corrosion and thermal shock resistance of TBC systems. *Mater. Sci. Forum* **2001**, *369–372*, 607–614. [CrossRef]

34. Mevrel, R.; Duret, C. Interdiffusion effects between protective coatings on superalloy substrates. In Proceedings of the NATO Advanced Workshop: Coatings for Heat Engines, Aquafredda di Maratea, Italy, 1–6 April 1984.

35. Huntz, A.M.; Boumaza, A.; Moulin, G. Improvement of the Oxidation Resistance of Superalloys by Low-Pressure, Plasma-Sprayed MCrAlYTa Coatings. I. *Oxid. Met.* **1988**, *30*, 141–183. [CrossRef]

36. Boudot, A. Propriétés des revêtements de protection haute température pour pales de turbine haute pression. Ph.D. Thesis, Institut National Polytechnique de Toulouse, Toulouse, France, 13 December 1999.

37. Dryepondt, S. Comportement et endommagement en fluage à haute température de parois minces en supralliage monocristallin MC2: Effets de l'oxydation et de l'application d'un revêtement MCrAlY. Ph.D. Thesis, Institut National Polytechnique de Toulouse, Toulouse, France, 25 March 2004.

38. Vialas, N. Etude de la détérioration par oxydation haute température et interdiffusion de systèmes revêtements/superalliage à base de nickel. Prévision de durée de vie. Ph.D. Thesis, Institut National Polytechnique de Toulouse, Toulouse, France, 15 November 2004.

39. Birks, N.; Meier, G.H.; Pettit, S. *Introduction to the High-Temperature Oxidation of Metals*; Cambridge University Press: Cambridge, UK, 2006; p. 338.

40. Mumm, D.R.; Evans, A.G.; Spitsberg, I.T. Characterization of a cyclic displacement instability for a thermally grown oxide in a thermal barrier system. *Acta Mater.* **2001**, *49*, 2329–2340. [CrossRef]

41. Vande Put, A.; Oquab, D.; Monceau, D. Characterization of TBC systems with NiPtAl or NiCoCrAlYTa bond coatings after thermal cycling at 1100 °C: A comparative study of failure mechanisms. *Mater. Sci. Forum* **2008**, *595–598*, 213–221. [CrossRef]

42. Allam, I.A.; Whittle, D.P.; Stringer, J. The oxidation behavior of CoCrAl systems containing active element additions. *Oxid. Met.* **1978**, *12*, 35–66. [CrossRef]

43. Mennicke, C.; He, M.Y.; Clarke, D.R.; Smith, J.S. The role of secondary oxide inclusions ("pegs") on the spalling resistance of oxide films. *Acta Mater.* **2000**, *48*, 2941–2949. [CrossRef]

44. Nijdam, T.J.; Marijnissen, G.H.; Vergeldt, E.; Kloosterman, A.B.; Sloof, W.G. Development of a Pre-Oxidation Treatment to Improve the Adhesion between Thermal Barrier Coatings and NiCoCrAlY Bond Coatings. *Oxid. Met.* **2006**, *66*, 269–294. [CrossRef]

45. Nijdam, T.J.; Sloof, W.G. Combined pre-annealing and pre-oxidation treatment for the processing of thermal barrier coatings on NiCoCrAlY bond coatings. *Surf. Coat. Technol.* **2006**, *201*, 3894–3900. [CrossRef]

46. Schulz, U.; Fritscher, K.; Ebach-Stahl, A. Cyclic behavior of EB-PVD thermal barrier coating systems with modified bond coats. *Surf. Coat. Technol.* **2008**, *203*, 449–455. [CrossRef]

47. Toscano, J.; Vaβen, R.; Gil, A.; Subanovic, M.; Naumenko, D.; Singheiser, L.; Quadakkers, W.J. Parameters affecting TGO growth and adherence on MCrAlY-bond coats for TBC's. *Surf. Coat. Technol.* **2006**, *201*, 3906–3910. [CrossRef]

48. Fisher, G.; Datta, P.K.; Burnell-Gray, J.S.; Chan, W.Y.; Soares, J.C. The effects of active element additions on the oxidation performance of a platinum aluminide coating at 1100 °C. *Surf. Coat. Technol.* **1998**, *110*, 24–30. [CrossRef]

49. Lau, H.; Leyens, C.; Schulz, U.; Friedrich, C. Influence of bondcoat pre-treatment and surface topology on the lifetime of EB-PVD TBCs. *Surf. Coat. Technol.* **2003**, *165*, 217–223. [CrossRef]

50. Guo, H.; Sun, L.; Li, H.; Gong, S. High temperature oxidation behavior of hafnium modified NiAl bond coat in EB-PVD thermal barrier coating system. *Thin Solid Films* **2008**, *516*, 5732–5735. [CrossRef]

51. Pint, B.A.; Haynes, J.A.; More, K.L.; Wright, I.G.; Leyens, C. Compositional effects on aluminide oxidation performance: Objectives for improved bond coats. In Proceedings of the Superalloys 2000, TMS, Warrendale, PA, USA, 17–21 September 2000.

52. Tawancy, H.M.; Sridhar, N.; Abbas, N.M.; Rickerby, D.S. Comparative performance of selected bond coats in advanced thermal barrier coating systems. *J. Mater. Sci.* **2000**, *35*, 3615–3629. [CrossRef]

53. Tawancy, H.M.; Mohamed, A.I.; Abbas, N.M.; Jones, R.E.; Rickerby, D.S. Effect of superalloy substrate composition on the performance of a thermal barrier coating system. *J. Mater. Sci.* **2003**, *38*, 3797–3807. [CrossRef]

54. Hesnawi, A.; Li, H.; Zhou, Z.; Gong, S.; Xu, H. Isothermal oxidation behaviour of EB-PVD MCrAlY bond coat. *Vacuum* **2007**, *81*, 947–952. [CrossRef]

55. Vialas, N.; Monceau, D. Substrate effect on the high temperature oxidation behaviour of a Pt modified aluminide coating. Part I: Influence of the initial chemical composition of the coating surface. *Oxid. Met.* **2006**, *66*, 155–189. [CrossRef]

56. Muamba, J.M.N.; Streiff, R. Sur l'effet de quelques éléments d'addition du substrat sur l'oxydation des revêtements d'aluminiures modifiés par le chrome déposés sur superalliages à base Nickel. *Mater. Sci. Eng. A* **1989**, *120*, 391–405. [CrossRef]

57. Huntz, A.M.; Boumaza, A.; Moulin, G.; Lebrun, J.L. Relation between the oxidation behaviour of superalloys protected by plasma sprayed NiCoCrAlYTa coatings and Metallurgical or Mechanichal parameters. In Proceedings of the Advanced Materials and Processing Techniques for Structural Applications, Paris, France, 7–9 September 1987.

58. Fox, P.; Tatlock, G.J. Effect of tantalum additions on oxidation of overlay coated superalloys. *Mater. Sci. Technol.* **1989**, *5*, 816–827. [CrossRef]

59. Gleeson, B.; Wang, W.; Hayashi, S.; Sordelet, D. Effects of Platinum on the Interdiffusion and oxidation Behavior of Ni-Al-Based Alloys. *Mater. Sci. Forum* **2004**, *461–464*, 213–222. [CrossRef]

60. Copland, E. *Thermodynamic Effect of Platinum Addition to beta-NiAl: An Initial Investigation*; Technical report NASA/CR-2005-213330; Case Western Reserve University: Cleveland, OH, USA, 1 January 2005.

61. Karlsson, A.M.; Xu, T.; Evans, A.G. The effect of the thermal barrier coating on the displacement instability in thermal barrier systems. *Acta Mater.* **2002**, *50*, 1211–1218. [CrossRef]

62. Tolpygo, V.K.; Clarke, D.R.; Murphy, K.S. Evaluation of interface degradation during cyclic oxidation of EB-PVD thermal barrier coatings and correlation with TGO luminescence. *Surf. Coat. Technol.* **2004**, *188–189*, 62–70. [CrossRef]

63. Shi, J.; Darzens, S.; Karlsson, A.M. Aspects of the morphological evolution in thermal barrier coatings and the intrinsic thermal mismatch therein. *Mater. Sci. Eng. A* **2005**, *392*, 301–312. [CrossRef]

64. Chen, M.W.; Glynn, M.L.; Ott, R.T.; Hufnagel, T.C.; Hemker, K.J. Characterization and modeling of a martensitic transformation in a platinum modified diffusion aluminide bond coat for thermal barrier coatings. *Acta Mater.* **2003**, *51*, 4279–4294. [CrossRef]

65. Balint, D.S.; Hutchinson, J.W. An analytical model of rumpling in thermal barrier coatings. *J. Mech. Phys. Solids* **2005**, *53*, 949–973. [CrossRef]

66. Evans, H.E.; Donaldson, A.T.; Gilmour, T.C. Mechanisms of Breakaway Oxidation and Application to a Chromia-Forming Steel. *Oxid. Met.* **1999**, *52*, 379–402. [CrossRef]

67. Schmutzler, H.J.; Viefhaus, H.; Grabke, H.J. The Influence of the Oxide/Metal Interface Composition on the Adherence of Oxide Layers on Metal Substrates. *Surf. Interface Anal.* **1992**, *18*, 581–584. [CrossRef]

68. Wright, I.G.; Pint, B.A.; Lee, W.Y.; Alexander, K.B.; Prübner, K. Some effects of metallic substrate composition on degradation of thermal barrier coatings. In Proceedings of the High Temperature Surface Engineering Conference, Edinburgh Scotland, UK, 22–24 September 1997.

69. Lee, W.Y.; Zhang, Y.; Wright, I.G.; Pint, B.A.; Liaw, P.K. Effects of Sulfur Impurity on the Scale Adhesion Behavior of a Desulfurized Ni-Based Superalloy Aluminized by Chemical Vapor Deposition. *Metall. Mater. Trans. A* **1998**, *29A*, 833–841. [CrossRef]

70. Haynes, J.A.; Zhang, Y.; Lee, W.Y.; Pint, B.A.; Wright, I.G.; Cooley, K.M. Effects of Platinum additions and sulfur impurities on the microstructure and scale adhesion behavior of single-phase CVD aluminide bond coat. In *Elevated Temperature Coatings: Science and Technology III, 1999*; The Minerals, Metals and Materials Society: Warrendale, PA, USA, 1999.

71. Haynes, J.A.; Lance, M.J.; Pint, B.A.; Wright, I.G. Characterization of commercial EB-PVD TBC systems with CVD (Ni,Pt)Al bond coatings. *Surf. Coat. Technol.* **2001**, *146–147*, 140–146. [CrossRef]

72. Cadoret, Y.; Monceau, D.; Bacos, M.; Josso, P.; Maurice, V.; Marcus, P. Effect of platinum on the growth rate of the oxide scale formed on cast nickel aluminide intermetallic alloys. *Oxid. Met.* **2005**, *64*, 185–205. [CrossRef]

73. Krupp, U.; Christ, H.J. Selective oxidation and internal nitridation during high-temperature exposure of single-crystalline nickel-base superalloys. *Metall. Mater. Trans. A* **2000**, *31*, 47–56. [CrossRef]

74. Orosz, R.; Krupp, U.; Christ, H.-J. Study of the oxide scale integrity on Ni-base alloy CMSX-4 during isothermal and thermal-cycling exposure. *Mater. Corros.* **2006**, *57*, 154–158. [CrossRef]

75. Raffaitin, A.; Crabos, F.; Andrieu, E.; Monceau, D. Advanced burner-rig test for oxidation-corrosion resistance evaluation of MCrAlY/superalloys systems. *Surf. Coat. Technol.* **2006**, *201*, 3829–3835. [CrossRef]

76. Subanovic, M.; Sebold, D.; Vassen, R.; Wessel, E.; Naumenko, D.; Singheiser, L.; Quadakkers, W.J. Effect of Manufacturing Related Parameters on Oxidation Properties of MCrAlY Bondcoats. *Mater. Corros.* **2008**, *59*, 463–470. [CrossRef]

77. Funkenbusch, A.W.; Smeggil, J.G.; Bornstein, N.S. Reactive Element-Sulfur Interaction and oxide scale adherence. *Metall. Trans. A* **1985**, *16A*, 1164–1166. [CrossRef]

78. Smialek, J.L. Adherent Al2O3 scales formed on undoped NiCrAl Alloy. *Metall. Trans. A* **1987**, *18A*, 164–167. [CrossRef]

79. Schumann, E.; Yang, J.C.; Graham, M.J. Direct observation of the interaction of yttrium and sulfur in oxidized NiAl. *Scr. Mater.* **1996**, *34*, 1365–1370. [CrossRef]

80. Craig, M.; Nicholls, J.R. *Private Communication*; Cranfield University: Cranfield, UK, 2008.